Chiral Plasmonics

Zhongyue Zhang

Abstract Chirality is a geometric feature, corresponding to the structures that cannot be brought to coincide with their mirror images. To discriminate the object chirality is critical and significant in many areas such as life science, chemistry and physics. Chiral plasmonic from two aspects including chiral near-fields and chiroptical effects in far-fields of nanostructures will be discussed. Chiral near-fields can be characterized by the optical chirality density. Chiroptical effects in far-fields can be analyzed by the transmission matrix. As for far-field chiroptical effects, circular birefringence (CB), circular dichroism (CD) and asymmetric transmission (AT) are frequently discussed. Additional, chiral biomolecules can change some characteristics of chiral nanostructures and thus can be used for chiral sensing. The sensor is easy to implement and is non-invasive to the analyte. Therefore, chiral plasmons have good application prospects in ultra-sensitive chiral molecular sensing. Plasmonic chirality is still evolving, and many phenomena and challenges remain undiscovered, such as circularly polarized luminescence, nonlinear chiral effects, chiral selective hot electron transfer, ultrafast detection, and chiral quantum optics. The research on plasmonic chirality plays a vital role in the future development of science and technology.

Keywords Chirality · Plasmonic · Chiral near-fields · Chiral far-fields · Circularly polarized light · Sensor

1 Chiral

Chirality splits the material world into left and right, ranging from small metal clusters of atoms to continuous metal surfaces and through the whole range of molecular materials, nanomaterials, hybrid materials, bio-materials and metamaterials. During

Z. Zhang (✉)
School of Physics and Information Technology, Shaanxi Normal University, Xi'an, China
e-mail: zyzhang@snnu.edu.cn

P. Yu et al. (eds.), *Plasmon-enhanced light-matter interactions*,
Lecture Notes in Nanoscale Science and Technology 31,
https://doi.org/10.1007/978-3-030-87544-2_1

Baltimore lectures on molecular dynamics and the wave theory of light, Lord Kelvin defined chirality as follows: "I call any geometric figure, or group of points, chiral, and say it has chirality if its image in a plane mirror, ideally realized, cannot be brought to coincide with itself" [1]. Chirality is a common natural phenomenon and exists widely in various fields of scientific research such as life chemistry. Chirality refers to the property that a structure and its mirror image cannot be completely overlapped, just as the left and right hands are mirror-symmetric but do not overlap, see Fig. 1. The word "chirality" is derived from a Greek word meaning "hand"; hence, a chiral object must have right or left handedness. These left- and right-handed structures are the mirror images of each other and are termed as enantiomers. In addition to hands, other living organisms have a large number of chiral components [2].

Chirality can be found everywhere in nature, ranging from micro-organisms and biomolecules to spiral galaxies, and plays an important role in the animal world. For example, the coloration of several butterfly wings (e.g., *Parides sesostris* and *Teinopalpus imperialis*) [3] and beetle exoskeletons (*Chrysina gloriosa*) is due to chiral photonic crystals [4]. In plants, the condensed fruit of Pollia exhibits iridescent color due to the chiral spiral photonic crystal. One chirality of limonene produces the smell of lemon, and the other chirality generates the smell of orange. The different performances of this smell have important consequences; for instance, in the fruit fly pheromone oil palm, the inertia of one hand attracts females, and the other hand attracts males [5]. In medicine, many drug molecules exhibit chirality. Only one enantiomer is suitable for disease treatment, and the other is non-functional or even toxic to humans [6]. All essential amino acids are chiral and have the same handedness, regardless of the equal energy of both chiral forms and the equal probability of their formation in an achiral environment. However, only one of these two occurs in nature and is the same for humans, animals, plants, and

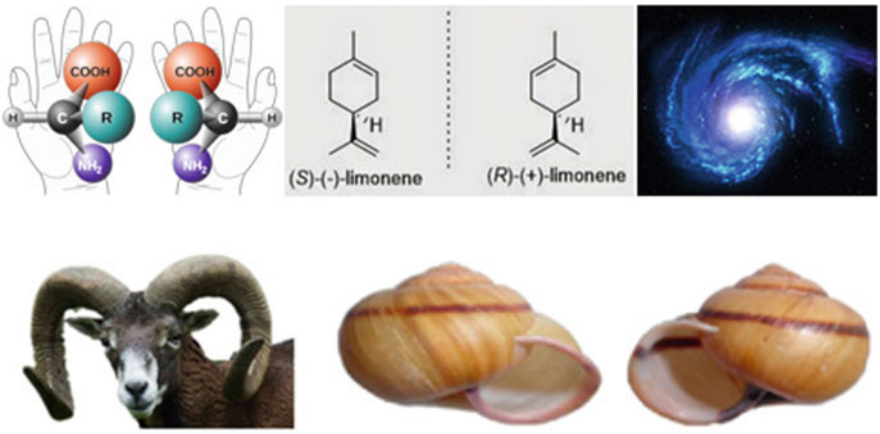

Fig. 1 Chiral objects

microorganisms [7]. Chirality appears to be a basic characteristic of living matter and perhaps even a requirement for life.

In 1848, Pasteur's experiments showed that the enantiomers of chiral molecules produce different results with polarized light. Therefore, polarized light is widely used to detect chirality. For example, the chiral structure can be detected by measuring the different absorption degrees of left circularly polarized (LCP) light and right circularly polarized (RCP) light. However, the chirality of structures in nature is extremely weak, and the interaction between chiral molecules and polarized light is not evident and thus cannot be accurately detected. With the development of nanostructure processing technologies, chiral plasmonic nanostructures or metasurfaces can be artificially manufactured to produce evanescent fields called "superchiral" plasmon near-fields, which have stronger chirality than many natural chiral systems because the artificial nanostructures structures can enhance chiral light–matter interactions [8–10].

The "superchiral" plasmonic near-field generated by the artificial chiral plasma structure can enhance the interaction between chiral light and matter. The chiral plasmonic structure maintains the "superchiral" near-field (also known as the chiral "hot spot"). One of the main research directions of chiral near-field is achiral nanostructures. 2D (planar) achiral nanostructures have attracted research attention because they can enhance local chirality by enhancing the magnetic or electric field and the nano-gap between plasmon and polymer. In general, planar achiral nanostructures can be fabricated by using electron beam lithography (EBL) and focused ion beam technology. 2D (planar) achiral nanostructures and chiral near-fields in 3D achiral nanostructures have also been widely investigated. The local chirality can be enhanced in 3D achiral nanostructures by spatially separating and enhancing magnetic or electric fields. Multiple EBL can be used to prepare 3D achiral nanostructures, the chirality of which is determined by the complex interaction between near-field interaction and phase retardation. Chiral near-fields can be characterized by the optical chirality density. The "superchiral" near-field exhibits different amplitudes and phases in the opposite case and can be used in engineering linear and nonlinear chiral interactions. For example, the "superchiral" near-field exhibits different amplitudes and phases under the excitation of RCP and LCP to manipulate the interaction of CP light materials [11]. In the interaction between quantum emitter and chiral plasmonic structure, the chiral hot spot is favorable for emission and has a specific chirality. The near-field chirality can be reflected in the far-field luminescence of the coupling dimmer, thus benefitting the luminescence of a specific hand.

Far-field chiral effect implies the interaction between polarized lights and artificial chiral plasmonic structures. The main research objects in far-field chirality are circular birefringence (CB), circular dichroism (CD), and asymmetric transmission (AT). CB refers to the optical rotation of polarization of the linearly polarized light transmitted through a chiral medium. Here, the rotation direction (clockwise or counterclockwise) is determined by the handedness of the chiral material. CD points to the differential absorption or transmission of RCP or LCP light. Chiroptical effects in far-fields can be analyzed by the transmission matrix. Assuming that a

given incident plane wave propagates in the $+z$ direction, the Jones matrix T_{circ} of circular polarization [12, 13] is described as follows:

$$T_{\text{circ}}^{+z} = \frac{1}{2}\begin{pmatrix} t_{xx} + t_{yy} + i\left(t_{xy} - t_{yx}\right) & t_{xx} - t_{yy} - i\left(t_{xy} + t_{yx}\right) \\ t_{xx} - t_{yy} + i\left(t_{xy} + t_{yx}\right) & t_{xx} + t_{yy} - i\left(t_{xy} - t_{yx}\right) \end{pmatrix} = \begin{pmatrix} t_{++} & t_{+-} \\ t_{-+} & t_{--} \end{pmatrix}, \tag{1}$$

where "x", "y", "+" and "–" are used to describe the polarized states of linearly x-polarized, linearly y-polarized, RCP light, and LCP light, respectively. Im(t_{xx}) and Re(t_{xx}) represent the real part and imaginary part of t_{xx}, respectively. The CD of the circularly polarized light is usually defined as follows:

$$\begin{aligned} CD^{+z} = T_{++} - T_{--} = |t_{++}|^2 - |t_{--}|^2 = \left[\text{Im}\left(t_{xx}\right) + \text{Im}\left(t_{yy}\right)\right]\left[\text{Re}\left(t_{xy}\right) - \text{Re}\left(t_{yx}\right)\right] \\ - \left[\text{Re}\left(t_{xx}\right) + \text{Re}\left(t_{yy}\right)\right]\left[\text{Im}\left(t_{xy}\right) - \text{Im}\left(t_{yx}\right)\right] \end{aligned} \tag{2}$$

AT is defined as the different RCP light to LCP light or LCP light to RCP light conversion efficiencies. In accordance with the above conditions, AT can also be represented by the transmission matrix.

The AT of the circularly polarized light is defined as follows [14]:

$$\begin{aligned} \Delta_{circ}^{+z} = T_{-+} - T_{+-} = |t_{-+}|^2 - |t_{-+}|^2 = \left[\text{Im}\left(t_{xx}\right) - \text{Im}\left(t_{yy}\right)\right]\left[\text{Re}\left(t_{xy}\right) + \text{Re}\left(t_{yx}\right)\right] \\ - \left[\text{Re}\left(t_{xx}\right) + \text{Re}\left(t_{yy}\right)\right]\left[\text{Im}\left(t_{xy}\right) - \text{Im}\left(t_{yx}\right)\right] \end{aligned} \tag{3}$$

2 Near-Field Chiral

The enhancement and handedness control of chiral near-fields are also crucial to improve the weak chiral effects of molecules and can be characterized by the optical chirality density, which can be quantified using the so-called optical chirality [15, 16]. In 1964, Lipkin proposed a quantity pseudo vector C [17],

$$C \equiv \frac{\varepsilon_0}{2}\mathbf{E} \cdot \nabla \times \mathbf{E} + \frac{1}{2\mu_0}\mathbf{B} \cdot \nabla \times \mathbf{B}, \tag{4}$$

where $\mathbf{E}$ and $\mathbf{B}$ represent electric field and magnetic field, respectively. ε_0 and μ_0 represent the vacuum dielectric constant and vacuum permeability, respectively. Lipkin's research also pointed out that C is a quantity stored in arbitrary electromagnetic waves and has no actual physical meaning.

In 2010, Tang and Cohen of Harvard university indicated that C describes the quantity of the chirality of the electromagnetic field and represents the efficiency of exciting the chiral signal of chiral molecules. For simplified calculation and understanding, C can be derived from Eq. (4) [15, 16, 18–22]:

$$C = -\frac{\varepsilon_0 \omega}{2} \mathrm{Im}\left(\mathbf{E} * \cdot \mathbf{B}\right), \tag{5}$$

which can be computed for monochromatic electromagnetic field. **E** and **B** are the complex electric and magnetic fields around the plasmonic nanostructures, respectively, and ω is their angular frequency.

According to the equation, parallel components of electric and magnetic fields can be obtained for fields with non-zero optical chirality. The maximum value of C for a plane wave is calculated from the circularly polarized light as follows:

$$C_{\mathrm{CPL}}^{\pm} = \pm \frac{\varepsilon_0 \omega}{2c} |\mathbf{E}|^2, \tag{6}$$

where $+$ and $-$ denote the LCP and RCP light, respectively, and c is the speed of light in a vacuum.

When Tang and Cohen proposed C, they assumed that the chirality of the local electromagnetic field needs be enhanced to improve the chiral signal of chiral molecules. They proposed that a strong C can be achieved at the standing wave node formed by circularly polarized light. In 2011, they experimentally verified a method to enhance chiral molecular signals [15].

To obtain a large optical chirality, researchers studied the influence of electromagnetic wave excitation of different polarization states on the optical chirality and the optical chirality with different metal nanostructures. According to Eq. (5), the magnitude of optical chirality is proportional to the imaginary part of **E***•**B**. This equation also provides two ways to enhance optical chirality. First is by reducing the angle between the electric and magnetic fields, and second is by increasing the electric or magnetic field. For the first case, the maximum value of optical chirality can be achieved when the directions between the electric and magnetic fields are parallel or anti-parallel as shown in Fig. 2.

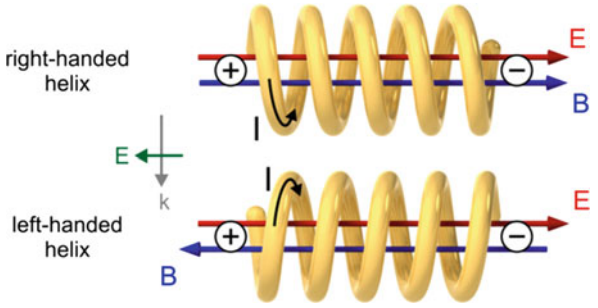

Fig. 2 Fundamental mode of a helical plasmonic nanoantenna exhibiting non-orthogonal electric and magnetic dipole moments. Given their nanostructure, the electric(red) and magnetic(blue) field vectors are mainly parallel, leading to a strong optical chirality and changes in the handedness of the structures, the relative orientation of vectors, and consequently the handedness of the chiral near-fields [26]

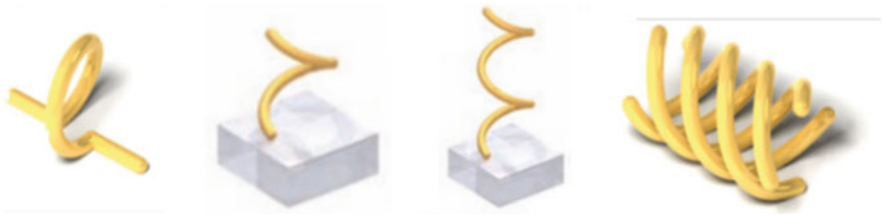

Fig. 3 Schematic of different helix nanostructures

Researchers recently proposed different plasmonic nanostructures to produce optical chirality and explored the reasons for the generation of optical chirality. Owing to the parallel directions of the electric field and the magnetic field in the spiral structure, the optical chirality is enhanced in the region surrounded by the wire. Therefore, different 3D nanostructures, such as loop-wire nanostructures [23–25] and multiple intertwined helices, have been employed to interact with circularly polarized light or linearly polarized light to generate optical chirality (Fig. 3) [11, 26]. The enhancement of optical chirality is due to the parallel electric and magnetic field components inside the spiral. The large pitch helix leads to a large volume that is enclosed by gold wires; hence, the multi-spiral nanostructure is used to improve the optical chirality as shown in Fig. 4. In general, the gold helix array is prepared by using laser to directly write photoresist and then electrochemically deposit the gold [25]. Preparing the precise helix nanostructure is extremely difficult. Therefore, the practical application of 3D devices is limited.

Layer-by-layer nanostructures composed of stacked and twisted planar nanostructures are designed to enhance local chirality depending on near-field enhancement. For this nanostructure, the enhancement of local chirality is strongest in the small gap between the upper and lower layer [18, 27, 28]. A layer-by-layer nanostructure composed of metal–dielectric–metal metasurface improves the local chirality through the interplay of the spatially separated and enhanced electric and magnetic fields with complementary profiles. In layer-by-layer nanostructures, one handed chiral field is obtained in the gap between the upper and lower layers, and the other handed chiral field surrounds the metal nanostructure [27]. The enhanced chiral near-field is located on the gap between the two nanostructured layers [27]. Unfortunately, it is difficult to use these strongly enhanced chiral fields in chiral molecular sensors. Layer-by-layer nanostructures are usually prepared through a multi-step advanced nanomanufacturing process. During the experiment, layer-by-layer nanostructures must be separated by dielectric layers, such as MgF_2 layers, so chiral molecules cannot be placed in areas where the chiral field is strongly enhanced between the interlayer spacing.

Planar polymer nanostructure illuminated with circularly polarization light is proposed to generate near-chiral fields for simplification. The chiral near-field is enhanced by boosting light–matter interaction. The improvement of local chirality originates from the simultaneous enhancement of magnetic and electric fields and

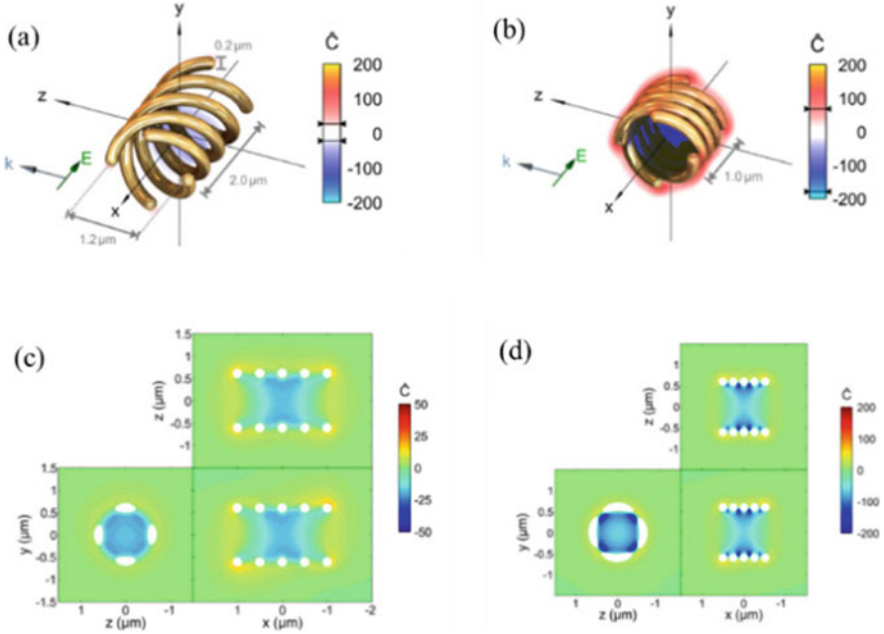

Fig. 4 (**a**) and (**b**) 3D optical chirality map for different pitch values showing chiral near-fields of one handedness in the whole interior of the nanostructure. (**c**) Optical chirality of slice plots for different pitch values. The slice plots confirm the confinement to the inner region [26]

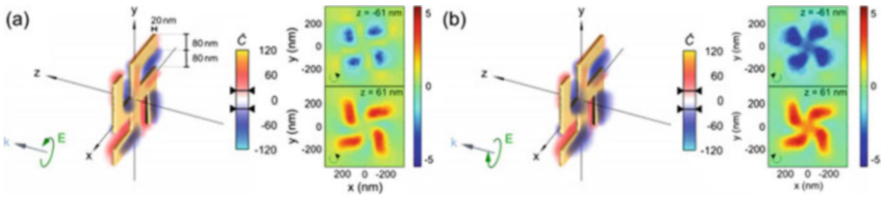

Fig. 5 Optical chirality enhancement by a planar gammadion structure illuminated with (**a**) LCP and (**b**) RCP at a wavelength of 2.01 µm [11]

their proper spatial overlap in the gap between polymer nanostructures as shown in Fig. 5 [29–33]. For example, optical chirality is generated around a swastika to achieve a chiral signal enhancement of 6 orders of magnitude. As a major difference, the gammadion shows both positive and negative values of optical chirality with similar absolute values, while for the helix the values corresponding to light with matching polarization are higher [20].

Optical chirality can be found around metal structures, and silicon (Si) nanoparticles also can generate large chiral electromagnetic fields. Si nanoparticles support electric and magnetic Mie resonances of substantial strength in the visible range of the electromagnetic spectrum [34–39]. These resonances originate from charge

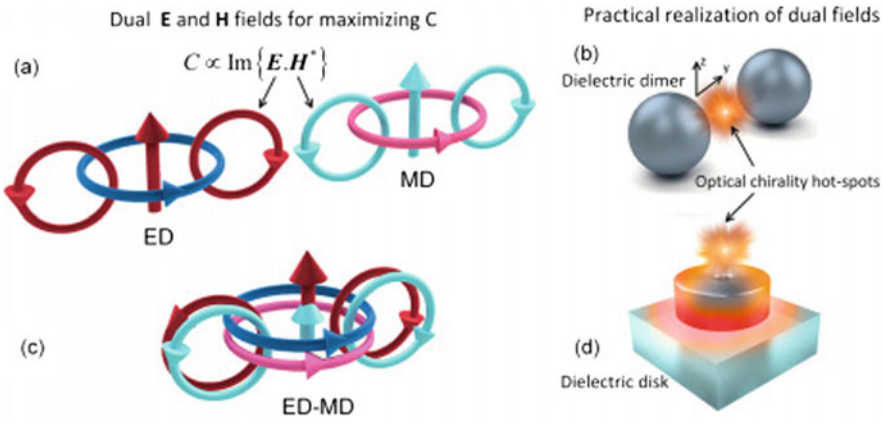

Fig. 6 (**a**) Duality of electromagnetic fields in a pair of electric and magnetic dipoles (ED and MD). The electric (red) and magnetic (blue) field lines of the electric dipole lie parallel with the corresponding magnetic (cyan) and electric (pink) field lines of the magnetic dipole. For comparison, similar color tones have been chosen for electric fields (red and pink) and magnetic fields (blue and cyan). (**b**) Realization of the dual dipoles in panel (**a**) by a dielectric nanodimer composed of two high refractive index spherical nanoparticles. (**c**) Overlapping electric and magnetic dual dipoles in a single nanoparticle by Kerker effect. (**d**) Holey dielectric disk could provide overlapped dipoles shown in panel (**c**) [36]

displacements in the high refractive index material. For Si nanodisks, the magnetic and electric dipole resonances are almost independently tunable via the aspect ratio [35, 36, 38, 40]. Solomon et al. investigated the near-field chirality enhancement in Si nanodisks with spectrally overlapping magnetic and electric dipole resonances as shown in Fig. 6 [41].

3 Far-Field Light-Matter Interactions

Artificial nanostructures provide a wealth of resources for designing customized optical responses. Different types of chiral structures have been designed with a common goal of using plasmons to enhance chiral responses. Under CPL illumination, artificial chiral metamaterials exhibit optical chirality due to the difference in refractive index and extinction coefficient of RCP and LCP. The chiral effects (CB, CD, and AT) are discussed for the far field of chiral plasmon and outlined in the following part of this chapter.

3.1 Circular Birefringence (CB)

CB refers to the optical rotation of polarization of the linearly polarized light transmitted through a chiral medium, in which the rotation direction (clockwise or counterclockwise) is determined by the handedness of the chiral material [42, 43]. Linearly polarized light can become circularly polarized light through a quarter glass and thus can be regarded as a combination of two circularly polarized lights (LCP and RCP). When RCP and LCP are transmitted in a chiral medium, linear polarization rotation occurs because their amplitudes are the same but their phase velocities are different. Kuwata–Gonokami et al. designed three sample—two enantiomorphs and an achiral pattern [31]. The measured achiral plasma structure and the rotation angle of the chiral plasma structure are shown in Fig. 7. Opposite rotation direction was observed with the left- and right-handed chiral structure, but no rotation was observed with the achiral structure.

Esposito et al. studied the hand optical properties of a 3D metal spiral system at light frequencies. A study focused on the optical activity of single nanowires and three nanowires under linear polarization and circular polarization and found that in the triple-helical nanowire configuration, the obtained pure CB can lead to a large optical activity of up to 8°, which is independent of the sample angle and extends in the visible light range in the 500 nm broad band [44].

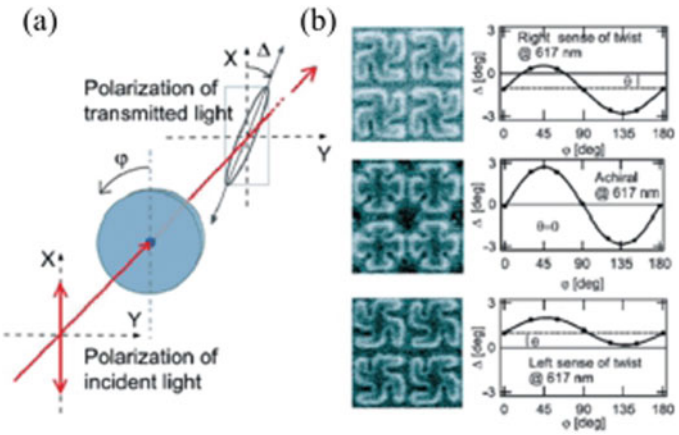

Fig. 7 (**a**) Schematic of CB measurement. (**b**) Optical rotation angles measured from plasmonic planar nanostructures with left-handedness, achiral geometry, and right-handedness [31]

3.2 Asymmetric Transmission

Circularly polarized light passing through the chiral structure is transformed into orthogonally polarized light. The conversion capacity of polarized light is called the transformation transmittance, and AT is the difference in transmittance between the two polarization states. For example, an RCP light is converted to an LCP light after passing through a chiral structure, and the quantitative relationship between the incoming RCP and the outgoing LCP is called the transformed transmittance (Fig. 8). When the incident light is LCP or RCP, the conversion transmittance is different. The conversion transmittance of the two kinds of polarized light is AT.

The AT of the circularly polarized light is defined as follows [46]:

$$AT = T_{-+} - T_{+-} = |t_{-+}|^2 - |t_{-+}|^2 = \left[\mathrm{Im}\left(t_{xx}\right) - \mathrm{Im}\left(t_{yy}\right)\right]\left[\mathrm{Re}\left(t_{xy}\right) + \mathrm{Re}\left(t_{yx}\right)\right] - \left[\mathrm{Re}\left(t_{xx}\right) + \mathrm{Re}\left(t_{yy}\right)\right]\left[\mathrm{Im}\left(t_{xy}\right) - \mathrm{Im}\left(t_{yx}\right)\right] \tag{7}$$

The AT effect was first discovered in metamaterials by Fedotov et al., who showed that this phenomenon is related to the direction of the light's propagation and the polarization state of the incident light. Under the strong interaction between electromagnetic waves and chiral metal structures, AT originates from the different polarized lights irradiated from the same polarized light in the opposite direction [47, 48]. This phenomenon is widely used in the design of polarization transformers and optical devices [49, 50]. At present, the AT effect of circularly polarized light excitation on many complex 3D has been studied. The AT effect of helical plasmonic nanostructures is the result of introducing spatial asymmetry into helical chiral nanostructures [13, 51].

The chiral plasmonic nanostructure of twist nanoslit-nanorod arrays can produce a remarkable AT effect (Fig. 9). Figure 10 illustrates that at the resonant wavelength, the spectra of T_{-+} and T_{+-} correspondingly present peaks and valleys, respectively, leading to a large AT effect. When the irradiation direction of polarized light is

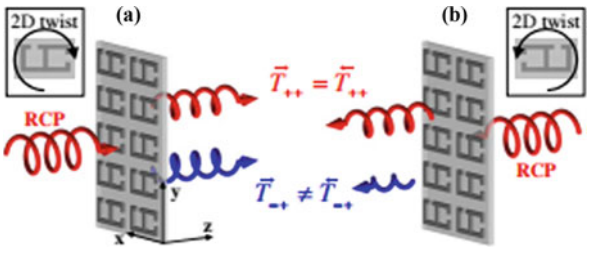

Fig. 8 (Color online) Asymmetric total transmission of a circularly polarized light incident on (**a**) front and (**b**) back side of a planar chiral metamaterial. The incident right-handed circularly polarized light (red spiral) is partially converted to the left-handed (blue spiral) polarization when propagating through the metamaterial [45]

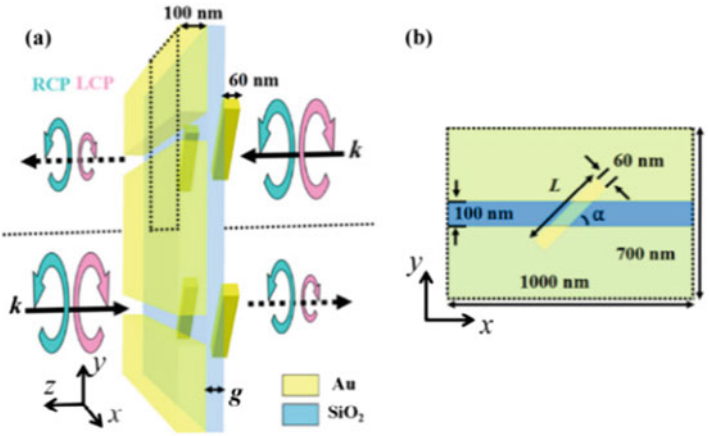

Fig. 9 (**a**) Schematic of TNNAs and (**b**) their unit cell with the associated geometric features [14]

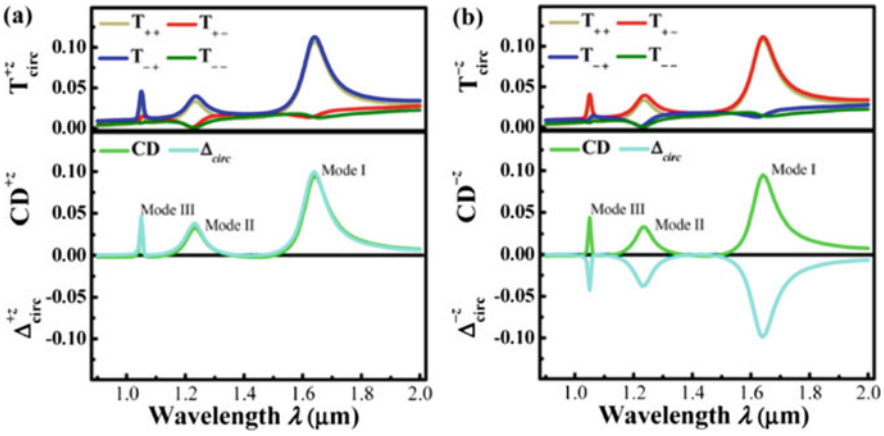

Fig. 10 Simulated (**T**)circ matrix, CD spectrum, and AT spectrum of TNNAs for $+z$-direction light excitation (**a**) and -z-direction light excitation (**b**). Three resonances labeled as mode I, II, and III [14]

changed, the spectra for T_{-+} and T_{+-} will produce reverse effects. The AT effect is highly dependent on the geometric parameters of the twist nanoslit-nanorod arrays.

The layer-by-layer structure is introduced to generate the AT effect of electromagnetic coupling between adjacent layers. Here, a composite chiral metamaterial composed of cut-wire pair and conjugated gammadion resonators is proposed (Fig. 11) [46]. Figure 11 shows that by changing the effective dielectric constant of composite chiral metamaterial medium, the electromagnetic behavior of the metamaterial can be controlled manually.

Spiral or multilayered chiral metamaterials are prepared using a complex process of bottom-up and top-down approach. Therefore, planar structures that produce AT

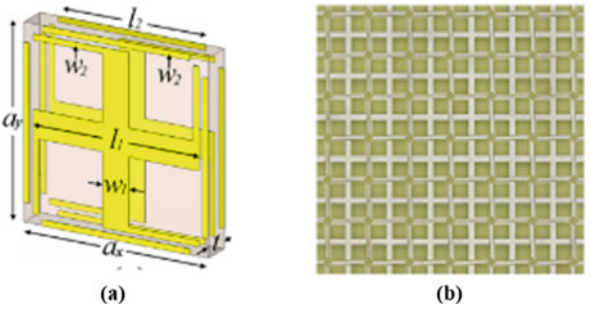

Fig. 11 (**a**) Scheme of a unit cell of the composite chiral metamaterial. (**b**) Photograph of the experimental sample [46]

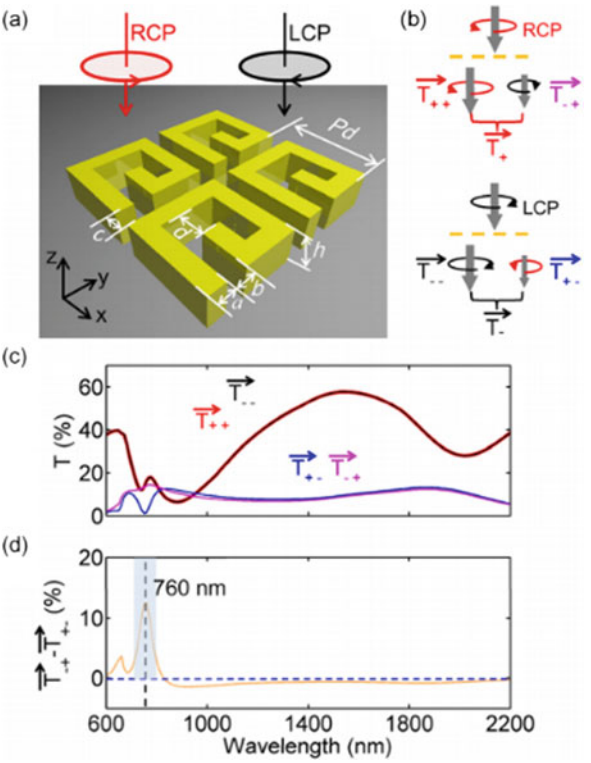

Fig. 12 (**a**) Design of the gold G-shaped chiral metamaterial suspended in air. (**b**) Illustration of transmission and polarization conversion of circularly polarized light partially directly transmit remaining the same handedness and partially convert to the opposite handed component. (**c**) Spectra for direct transmission T_{++},T_{--}, circular polarization conversion T_{-+}, T_{+-}, and (**d**) circular polarization conversion dichroism $T_{-+}-T_{+-}$ [52]

effect, such as G-shaped structures, coupled cleavage resonators, and chiral fish-scale structures, have become research hotspots [52] (Fig. 12).

Broadband AT can be achieved in the spectral range using 2D monolayer spiral metamaterials. The AT effect with a bandwidth greater than 940 nm in the range of 965–1905 nm is realized by increasing the winding number of the element atoms (Fig. 13). Electric and MD have opposite chirality as incident lights. They radiate the counter-handed transmitted field component, which leads to the conversion from the incident RCP light to the transmitted LCP light.

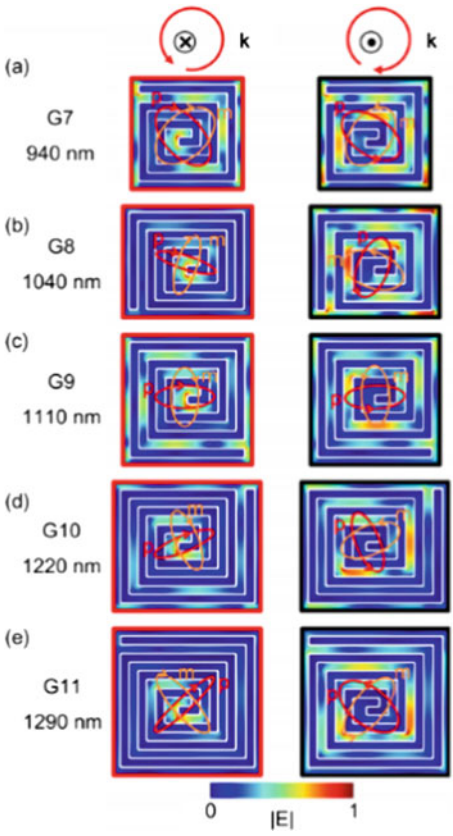

Fig. 13 Electric field magnitude |E| distributions excited by RCP light incident from opposite sides are presented by grey maps for structures G7 (**a**), G8 (**b**), G9 (**c**), G10(**d**), and G11 (**e**). Propagating directions of lights are indicated by the light vectors **k**. The induce effective electric **p** and magnetic m dipoles in individual elements are given by solid black (red online) and grey (orange online) lines, respectively [52]

In contrast to the above protruding planar structures, metal films with nanoslits are easily and directly powered on as specific electrodes [53]. Such films can confine localized electric fields along the nanoslits (Figs. 14 and 15). Therefore, the design of nanoslits in thin films can aid in clarifying the mechanism of this effect and may show promising applications.

Tilted rectangular nanohole arrays (Fig. 16) in a square lattice have been proposed to produce AT effect. The AT properties of the tilted rectangular nanohole strongly depend on structural parameters, such as width, length, thickness, and tilted angle of tilted rectangular nanohole.

When the tilted rectangular nanohole is irradiated by circularly polarized light, the LSP and SPP appear around the tilted rectangular nanohole, thus producing the AT effect. In particular, the mechanism of SPPs provides another means to achieve AT effect, that is, when the array period matches the wavelength of the SPPs.

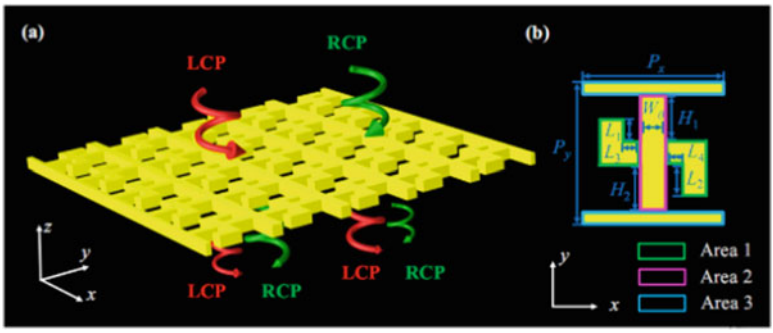

Fig. 14 (**a**) Schematic model of connected gammadion-shaped nanostructure arrays and (**b**) their unit cell with the associated parameter definition [54]

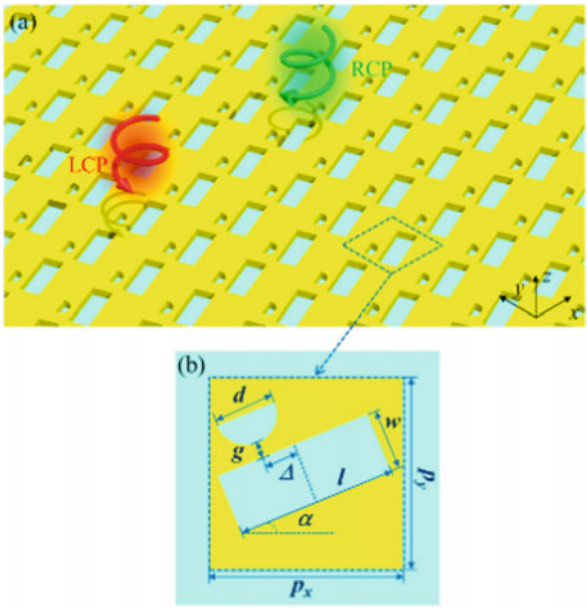

Fig. 15 (**a**) Schematic model of nanostructure arrays and (**b**) their unit cell with the associated parameter definition [55]

3.3 Circular Dichroism (CD)

CD points to the differential absorption or transmission of RCP or LCP light [57]. This parameter can identify enantiomers and is important in life science, analytical chemistry, biochemistry, and medical science. Compared with natural chiral molecules, such as DNA and proteins, artificially manufactured chiral plasmonic

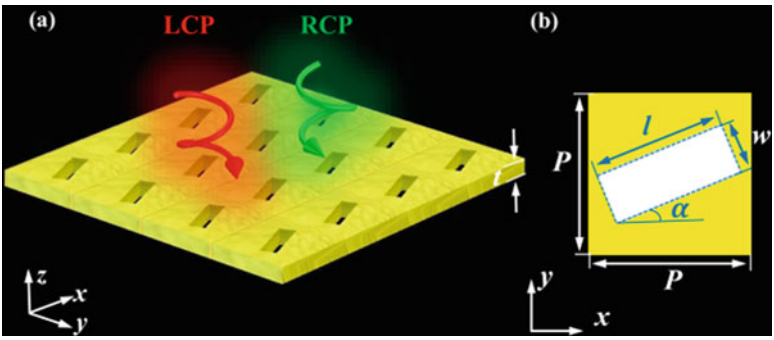

Fig. 16 (**a**) Schematic of tilted rectangular nanohole arrays with perforated gold film and (**b**) their unit cell with the associated geometric features [56]

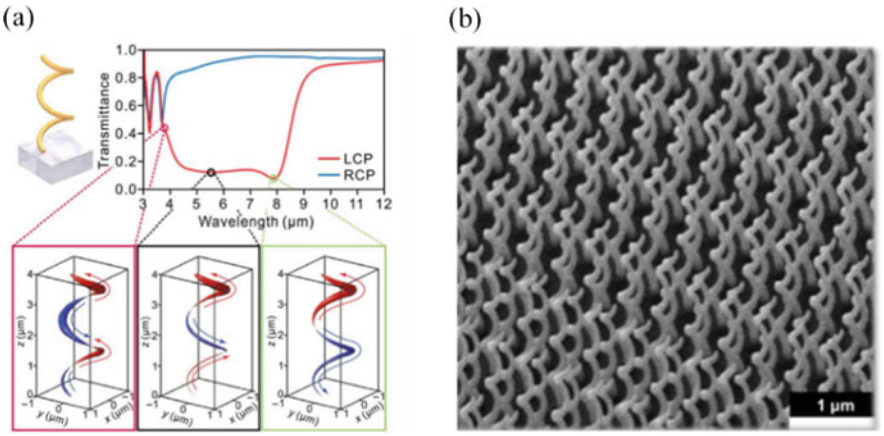

Fig. 17 (**a**) Simulated transmittance spectra and plasmonic modes of a metallic spiral with two pitches. The structures basically block LCP light while transmitting RCP light nearly without loss [25]. The observed plasmonic modes extend over the entire structure, thus being strongly handed themselves. (**b**) Platinum helices produced by focused ion and electron beam deposition [59]

nanostructures show larger CD response. Different strategies have been adopted to enhance the CD signal and improve detection sensitivity.

The helix is a typical chiral geometric structure and has attracted attention for CD effect enhancement. In 1940s, Kraus invented the helical antenna [58], which is widely used today. Gansel et al. proved that the vibration mode of the plasmon helix is a standing wave type. Figure 17a shows that the structures basically block LCP light while transmitting RCP light nearly without loss. Each of these modes has a distinct handedness and thus predominately interacts with the light of the same handedness [25]. Esposito et al. used focused ions and electron beam-induced deposition to prepare platinum helix with up to 22% CD in the visible spectrum as shown in Fig. 17b [59]. Helical nanostructures typically result in CD spectra in the

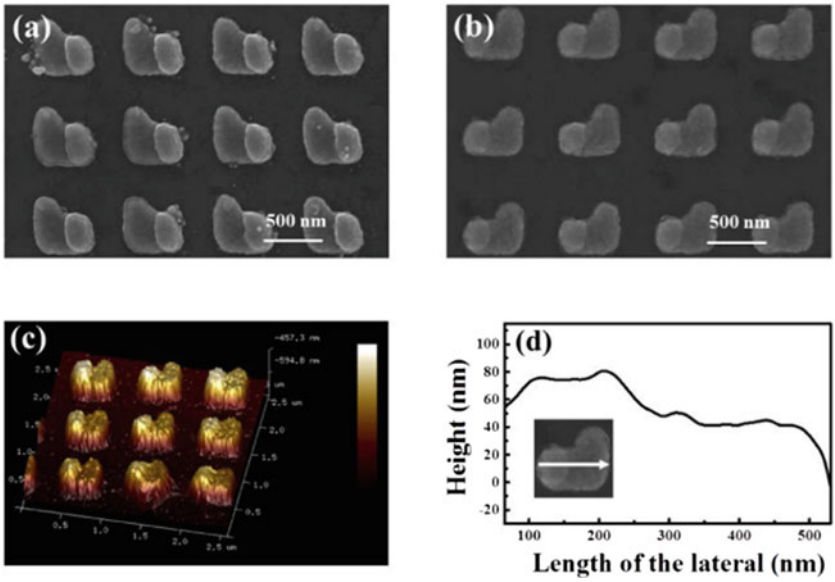

Fig. 18 (**a**) SEM images and 3D AFM measurement of nanostructure. (**a**), (**b**) SEM images of LH- and RH-LSNDH arrays; (**c**) 3D AFM image of RH-LSNDH arrays; (**d**) height profile of LSNDH in panel along the cross-section line shown in the bottom left corner. The height of the arm with coverage layer height is approximately 60 nm [67]

visible and NIR regions; however, their cumbersome preparation process hinders their application.

Given that the helical structure is difficult to prepared, scientists have proposed different kinds of 3D structures to enhance the CD effect. Zhao et al. used the colloidal monolayer technology of PS beads and the glancing angle deposition (GLAD) technology to create 3D nanostructures. Helically stacked plasmonic layers [60] and fan-shaped nanostructures [61] (Fig. 18a) have partial characteristics of helical. By using a similar technique, Zhang et al. designed L-shaped chiral nanostructures with different thicknesses of the two slices [62], U-shaped tilted multilayer structures [60], and chiral L-shaped nanostructure added with an achiral nanorod [63]. In the U-shaped tilted multilayer structures, the thickness of the SiO_2 film served as the basis to control the phase difference [60]. The CD signal of the U-shaped 3D structure increases with the phase difference. A chiral L-shaped nanostructure at the bottom is coupled with an achiral nanorod acquiring different positions in the top layer with respect to the long and/or short arm of the chiral L-shaped nanostructure at the bottom layer [63]. The metastructure generates a giant CD signal resulting from the strong coupling of the multipolar and dipolar resonant modes on the two layers.

In addition to providing a certain spiral characteristic for the structure, other strategies can be employed to enhance the CD effect. In the Fabry–Perot (F–P)

cavity strategy, the CD effect can be enhanced by multiple reflections inside the dielectric spacer [64, 65]. Metal–insulator–metal (MIM) structures with periodic ordered patterns offer rich optical responses and CD effects from the coupling between the localized plasmon of nanoparticles and the surface plasmon mode sustained by the underlying metallic layer [66]. The CD effect can also be improved by the direct coupling of the upper metal and the lower metal. For example, L-shaped planar silver nanostructures were prepared using EBL and normal electron beam deposition, and the GLAD method was used to partially cover one arm of the L-shaped nanostructure as shown in Fig. 18 [67]. Simulations revealed that the height difference in the two arms of the L-shaped NDH causes a variation in the polarization directions of the LCP and RCP incident light, thereby generating CD effects.

In addition to the 3D nanostructures, the CD effect is also found in the layer-by-layer nanostructure. Decker et al. prepared chiral metamaterial structure composed of right-handed twisted gold crosses (Fig. 19a). Although single-layer crosses are not chiral, they develop chirality along the direction perpendicular to their surface when placed on top of another layer of cross and rotated on an angle [68]. Another typical structure is the U-shaped nanostructure, which is also called split ring resonator (SRR). Decker et al. prepared an array of SRRs, where the unit cell is made of four SRRs each rotated at 90° with respect to its neighbors as shown in Fig. 19b [69].

Compared with 3D and layer-by-layer structures, the chirality of the planar structure is relatively small because the former are a real chiral structure, whereas the chirality of the planar structure is mainly caused by the physical difference between the air sample and the sample–matrix interface. Although the chirality of

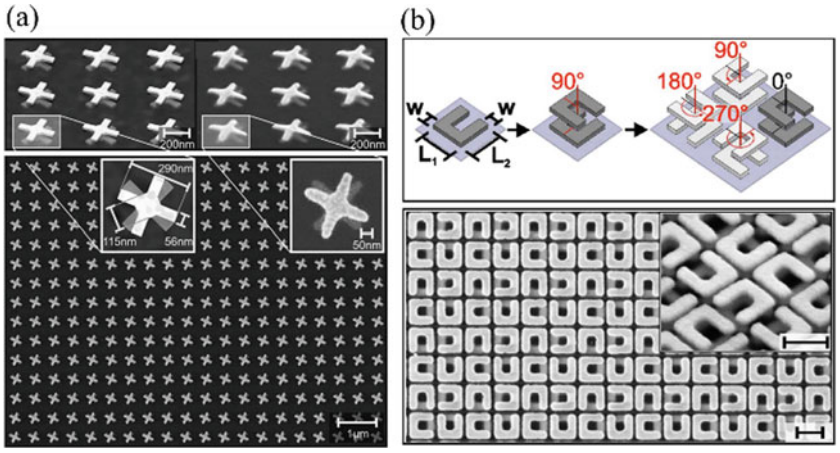

Fig. 19 (**a**) Scheme of the chiral metamaterial structure composed of right-handed twisted gold crosses [68]. (**b**) Schematic diagram and SEM image of a four-fold rotationally symmetric double-layer composed of U-shaped gold nanostructures [69]

planar structures is relatively small, planar chiral nanostructures can be combined with other materials through modern nanomanufacturing technology to open up new possibilities. For example, introducing 2D materials to the planar structure can produce strong surface electric field and lead to large CD effects [70]. For the most basic array composed of a single chiral structure, such as S-shaped [71] and gammadion-shaped [72] nanostructure, the CD effect occurs due to the LSP on the different parts of structures. Another common technique is the coupling between the two structures and the enhancement of the CD effect through the gap plasmon. The CD signal of planar heptamer gold nanostructures is due to the coupling between light and dark collective modes achieved by rotating the peripheral hexamer [29], thus providing large local electromagnetic field enhancements and strong near-field couplings.

4 Sensor

Chiral biomolecules are one of the basic units of life. Certain chiral molecular units are also important components of many drugs. Therefore, the detection and sensing of chiral molecules are particularly important. However, the weak chiral response of chiral molecules complicates the process of chiral molecular sensing. Chiral biomolecules can change some characteristics of chiral nanostructures and thus can be used for chiral sensing. This technique is easy to implement and is non-invasive to the analyte. Therefore, chiral plasmons have good application prospects in ultra-sensitive chiral molecular sensing.

The wavelength shift of chiral molecules can be achieved through the superchiral electromagnetic field capability generated by artificial chiral plasmonic nanostructures [73–78]. For example, the superchiral electromagnetic field generated by the optical excitation of plasmonic plane chiral metamaterial (PCM) is a highly sensitive probe of chiral supramolecular structure [78]. The PCM is prepared into a gamma-ray structure. The CD spectrum of the structure produces three resonance modes, which correspond to different localized surface plasmon resonances (LSPRs). When biomolecules are adsorbed, the gamma structure can be strongly coupled with chiral molecules. The refractive index change of LSPRs will displace the LSPRs, thereby changing the CD spectrum of PCM. The asymmetry of the refractive index of biomolecules can be extracted by the deviation of the CD spectrum. Therefore, the chirality of biomolecules can be judged, and the detection sensitivity can be greatly improved.

A low-cost and high-efficiency tilt angle deposition method has also been used to prepare large-area chiral molecular probes (in Fig. 20a) [76]. The plasmonic chiral conic nanoshell metallic nanostructure (CCNM), which is composed of three nanoshells of different heights, is synthesized by varying the incidence and orientation angles of deposition to achieve symmetry breaking. Such a conic nanoshell nanostructure can couple the incident light into the nanostructure, thus reducing the reflection and localizing the electromagnetic energy inside the nanoshell. This

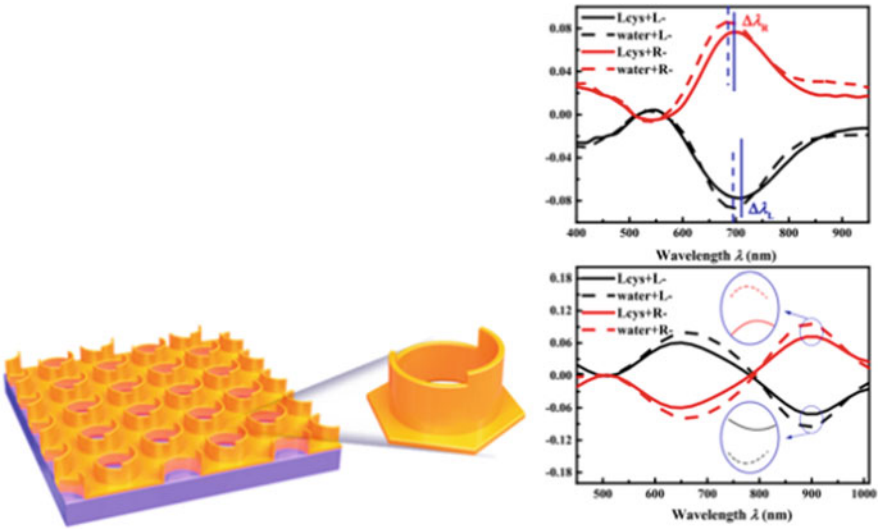

Fig. 20 (**a**) CCNM Structural diagram (**b**) experimental and simulated ΔT spectra of the R-CCNM and the L-CCNM in water (dashed line) and chiral L-cys solution (solid line). The shift of resonant peak from water to the chiral solution is defined as Δλ, and the inset is the amplified shift of the CD peak

structure can also achieve CD spectrum shift by adsorbing chiral molecules (in Fig. 20b) for chiral molecule detection.

In 1966, Bosnich showed that chiral molecules can induce CD at the absorption lines of achiral molecules with which they are closely interacting [79]. Induced circular dichroism (ICD) is the one which results from the interaction of chiral molecules with metal nanostructures, in this case the CD signal of chiral molecules lies between ultraviolet and visible bands. With monolayer inscribed graphene dual-rings arrays (IGDAs) and chiral molecular structures as examples, the ICD from the interaction of chiral molecules and metal nanostructures is shown in Fig. 21a, b. Figure 21c shows the T_{++} of chiral molecules, outer rings, inner rings, and IGDAs with chiral molecules. The T_{++} of chiral molecules, inner rings, and outer rings presents three resonant dips in $\lambda_0 = 0.192$ μm, $\lambda_{IR} = 22.084$ μm, and $\lambda_{OR} = 41.131$ μm, respectively. When the IGDAs composed of the inner ring and the outer ring are immersed in a chiral molecule, their transmission spectrum (black line) T_{++} ranges from 10 μm to 60 μm band and shows nine new resonance dips represented by λ_i (i from "1" to "9"). At the wavelength λ_i, the newly appeared CD signal is called an induced CD signal. Researchers have experimentally and theoretically studied the interaction between chiral molecules and metal nanostructures to induce molecular chiral signals from the ultraviolet band to the visible light band.

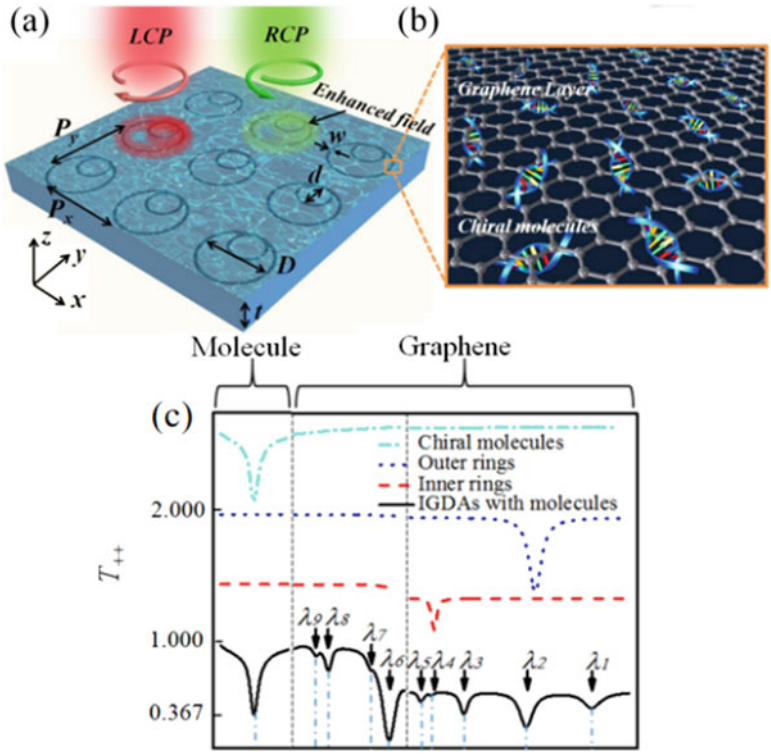

Fig. 21 (**a**) Schematic of IGDAs immersed in chiral molecular solution and parameters definition; (**b**) the zoom cell presenting grapheme layer and chiral molecules; (**c**) T_{++} of chiral molecules, outer rings, inner rings, and IGDAs with chiral molecules [80]

In theory, the plasma-enhanced CD is an ideal choice for detecting the chirality of molecules [81, 82] and can achieve the chirality detection of single-layer molecules or single molecules. As shown in Fig. 22a–c, gold nanorod dimers with chiral molecules fixed in the gap have stronger effect on resonance and non-resonance CD signals. For a gap size of 5 nm, an enhancement factor of up to 3000 can be expected. The CD enhancement factor is related to the average electric field in the gap [83]. Figure 22d–f shows that the CD spectra of individual chiral molecules and IGDAs with chiral molecules almost overlap at $\lambda_0 = 0.192$ μm. However, the CD spectrum of IGDAs with chiral molecules exhibits new CD signals in the microwave band. The wavelength of these newly emerged CD signals is almost the same as the resonance wavelength of IGDAs. Hence, the resonance valley is determined by the chiral molecule.

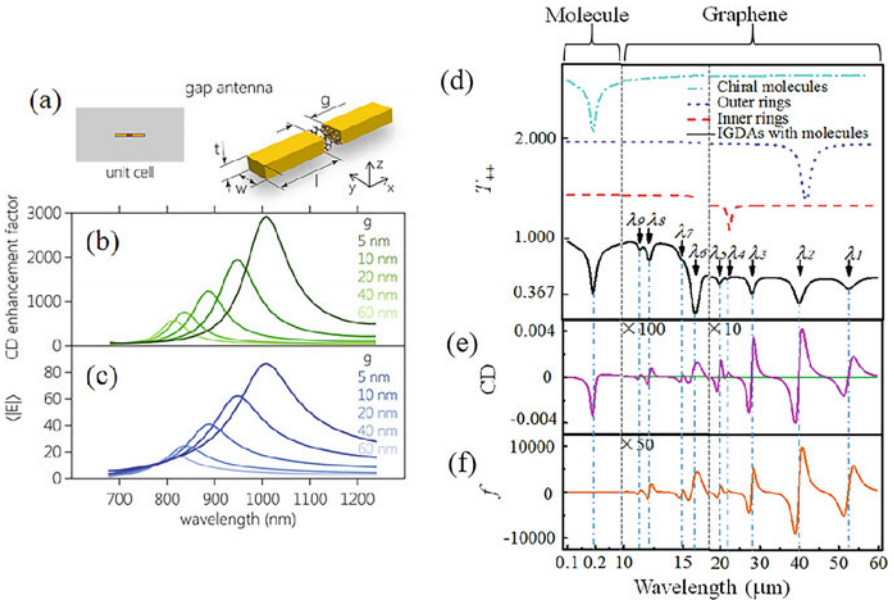

Fig. 22 (**a**) Schematics of gold nanorod dimer with chiral molecules immobilized in the gap; (**b**) calculated CD enhancement factor for different gap size; (**c**) corresponding values of average electric field in the gap volume [85]. (**d**) T_{++} of chiral molecules, outer rings, inner rings, and IGDAs with chiral molecules; (**e**) CD spectra of chiral molecules alone (green line) and with IGDAs (magenta line); (**f**) the CD enhancement factor f as the ratio between the values of magenta line and with green line [81]

Experimental analysis of the formation of chemical bonds revealed that molecular charges can be transferred to surface plasmonic nanostructures [85]. In addition, optical activity can be enhanced or inhibited through specially tailored nanostructures to customize optical activity [86]. As shown in Fig. 23, the formed achiral nanoparticles, namely, gold/silver core/shell nanocubes, can be used as chiral additional molecules of the plasma and can provide 2 orders of magnitude CD enhancement in the near visible region [87].

Chiral molecular sensing is important and is currently achieved by moving the chiral CD spectrum or inducing CD production. The self-assembly of plasmonic nanostructures triggered by chiral molecules is a promising method for chiral molecular sensing [74]. Therefore, chiral plasmons play an important role in chiral molecular sensing. Many possibilities and aspects worth studying remain unexplored.

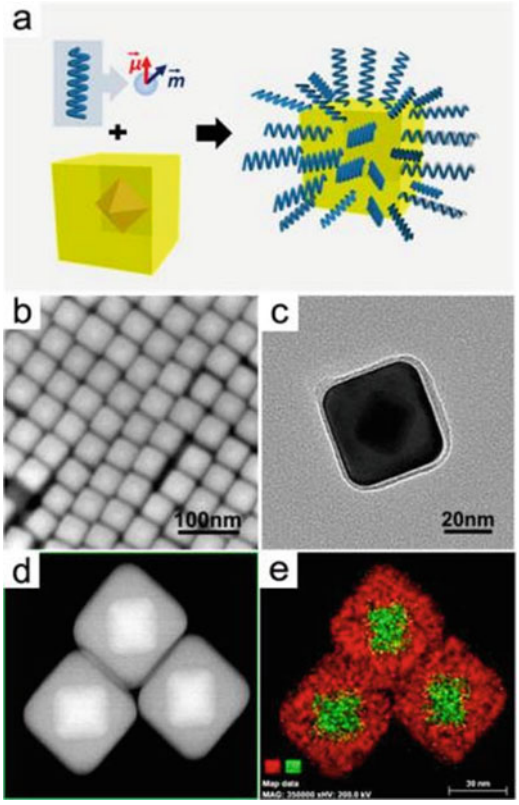

Fig. 23 Plasmonic nanoparticle with chiroptical activity, based on silver nanocube and DNA. (**a**) Design of "individual plasmonic chiral nanoparticle" using a gold/silver (Au/Ag) core−shell nanocube (namely, Ag NC) surface-functionalized with chiroptical molecules (e.g., DNA), theoretically expected to exhibit a plasmon- CD response. Structural characterizations of single-strand (ss) DNA-functionalized Ag NCs (**b**−**e**). (**b**) Low-magnification scanning electron microscopy (SEM) and (**c**) trans-mission electron microscopy (TEM) images show size and shape uniformity of nanocubes with edge length of 42 ± 2 nm. (**d** and **e**) Scanning transmission electron microscopy (STEM) and the corresponding energy dispersive X-ray (EDX) mapping images showing that the nanocube is made of an octahedral Au core embedded with thick cubic shell of Ag [87]

5 Outlook

Plasmonic chirality shows many unique characteristics in the near and far fields and provides many exciting possibilities for the sensing of molecular chirality for chirality improvement and CD induction. Different chiral metal nanostructures, such as 3D, multi-layer, and planar chiral nanostructures, have been prepared using some advanced methods, including top-down and bottom-up technology, and can be combined with different chiral molecules for various sensors. However, a tunable sensor is necessary for practical application. On the basis of their continuous

maturity in scientific research and their high electron mobility, 2D materials have shown good effects in the design and regulation of metal structures [88, 89]. Recent research indicated that surface plasmon effects can also be excited in semiconductors, such as InAS nanowires and carbon nanotubes [90–92]. Given the electrical tunability of semiconductors, electric fields can be used to control the light field and achieve the tunability of plasmons and chirality. These ideas can serve as references for the design of molecular sensors based on plasmonic chiral nanostructures in the future and provide new ideas for the generation of plasmonic chirality.

Plasmonic chirality is still evolving, and many phenomena and challenges remain undiscovered, such as circularly polarized luminescence, nonlinear chiral effects, chiral selective hot electron transfer, ultrafast detection, and chiral quantum optics. The research on plasmonic chirality plays a vital role in the future development of science and technology.

References

1. Thomson, W., & Kelvin, B. (2010). Lecture Xi. In *Baltimore lectures on molecular dynamics and the wave theory of light* (pp. 122–134). Cambridge University Press.
2. Hutt, A. J., & Tan, S. C. (1996). Drug chirality and its clinical significance. *Drugs, 52*(Suppl 5), 1–12.
3. Sharma, V., et al. (2009). Structural origin of circularly polarized iridescence in jeweled beetles. *Science, 325*(5939), 449–451.
4. Vignolini, S., et al. (2013). Analysing photonic structures in plants. *Journal of the Royal Society Interface, 10*(87), 20130394.
5. Coric, I., & List, B. (2012). Asymmetric spiroacetalization catalysed by confined Bronsted acids. *Nature, 483*(7389), 315–319.
6. Du, W., et al. (2019). Chiral plasmonics and enhanced chiral light-matter interactions. *Science China Physics, Mechanics & Astronomy, 63*(4), 1–11.
7. Collins, J. T., et al. (2017). Chirality and chiroptical effects in metal nanostructures: Fundamentals and current trends. *Advanced Optical Materials, 5*(16), 1700182.
8. Yoo, S., & Park, Q. H. (2019). Metamaterials and chiral sensing: A review of fundamentals and applications. *Nanophotonics, 8*(2), 249–261.
9. Luo, Y., et al. (2017). Plasmonic chiral nanostructures: Chiroptical effects and applications. *Advanced Optical Materials, 5*(16), 1700040.
10. Hentschel, M., et al. (2017). Chiral plasmonics. *Science Advances, 3*(5), e1602735.
11. Schäferling, M., et al. (2012). Tailoring enhanced optical chirality: Design principles for chiral plasmonic nanostructures. *Physical Review X, 2*(3), 031010.
12. Pfeiffer, C., et al. (2014). High performance bianisotropic metasurfaces: Asymmetric transmission of light. *Physical Review Letters, 113*(2), 023902.
13. Gansel, J. K., et al. (2010). Gold helix photonic metamaterials: A numerical parameter study. *Optics Express, 18*(2), 1059–1069.
14. Wang, Y., et al. (2016). Co-occurrence of circular dichroism and asymmetric transmission in twist nanoslit-nanorod arrays. *Optics Express, 24*(15), 16425–16433.
15. Tang, Y., & Cohen, A. E. (2011). Enhanced enantioselectivity in excitation of chiral molecules by superchiral light. *Science, 332*(6027), 333–336.
16. Tang, Y., & Cohen, A. E. (2010). Optical chirality and its interaction with matter. *Physical Review Letters, 104*(16), 163901.

17. Lipkin, D. M. (1964). Existence of a new conservation law in electromagnetic theory. *Journal of Mathematical Physics, 5*(5), 696–700.
18. Schäferling, M., et al. (2016). Reducing the complexity: Enantioselective chiral near-fields by diagonal slit and mirror configuration. *ACS Photonics, 3*(6), 1076–1084.
19. Schaeferling, M., Yin, X., & Giessen, H. (2012). Formation of chiral fields in a symmetric environment. *Optics Express, 20*(24), 26326–26336.
20. Meinzer, N., Hendry, E., & Barnes, W. L. (2013). Probing the chiral nature of electromagnetic fields surrounding plasmonic nanostructures. *Physical Review B, 88*(4), 041407.
21. Hendry, E., et al. (2012). Chiral electromagnetic fields generated by arrays of nanoslits. *Nano Letters, 12*(7), 3640–3644.
22. Davis, T. J., & Hendry, E. (2013). Superchiral electromagnetic fields created by surface plasmons in nonchiral metallic nanostructures. *Physical Review B, 87*(8), 085405.
23. Tretyakov, S. A., et al. (1996). Analytical antenna model for chiral scatterers: Comparison with numerical and experimental data. *IEEE Transactions on Antennas and Propagation, 44*, 1006–1014.
24. Rockstuhl, C., et al. (2009). Optical activity in chiral media composed of three-dimensional metallic meta-atoms. *Physical Review B, 79*(3), 035321.
25. Gansel, J. K., et al. (2009). Gold helix photonic metamaterial as broadband circular polarizer. *Science, 325*(5947), 1513–1515.
26. Schäferling, M., et al. (2014). Helical Plasmonic nanostructures as prototypical chiral near-field sources. *ACS Photonics, 1*(6), 530–537.
27. Rui, G., et al. (2019). Symmetric meta-absorber-induced superchirality. *Advanced Optical Materials, 7*(21), 1901038.
28. Decker, M., et al. (2007). Circular dichroism of planar chiral magnetic metamaterials. *Optics Letters, 32*(7), 856–858.
29. Zu, S., Bao, Y., & Fang, Z. (2016). Planar plasmonic chiral nanostructures. *Nanoscale, 8*(7), 3900–3905.
30. Papakostas, A., et al. (2003). Optical manifestations of planar chirality. *Physical Review Letters, 90*(10), 107404.
31. Kuwata-Gonokami, M., et al. (2005). Giant optical activity in quasi-two-dimensional planar nanostructures. *Physical Review Letters, 95*(22), 227401.
32. Horrer, A., et al. (2020). Local optical chirality induced by near-field mode interference in achiral plasmonic metamolecules. *Nano Letters, 20*(1), 509–516.
33. Eftekhari, F., & Davis, T. J. (2012). Strong chiral optical response from planar arrays of subwavelength metallic structures supporting surface plasmon resonances. *Physical Review B, 86*(7), 075428.
34. van de Groep, J., & Polman, A. (2013). Designing dielectric resonators on substrates: Combining magnetic and electric resonances. *Optics Express, 21*(22), 26285–26302.
35. Staude, I., et al. (2013). Tailoring directional scattering through magnetic and electric resonances in subwavelength silicon Nanodisks. *ACS Nano, 7*(9), 7824–7832.
36. Mohammadi, E., et al. (2019). Accessible superchiral near-fields driven by tailored electric and magnetic resonances in all-dielectric nanostructures. *ACS Photonics, 6*(8), 1939–1946.
37. García-Etxarri, A., & Dionne, J. A. (2013). Surface-enhanced circular dichroism spectroscopy mediated by nonchiral nanoantennas. *Physical Review B, 87*(23), 235409.
38. Butakov, N. A., & Schuller, J. A. (2016). Designing multipolar resonances in dielectric metamaterials. *Scientific Reports, 6*, 38487.
39. Bakker, R. M., et al. (2015). Magnetic and electric hotspots with silicon nanodimers. *Nano Letters, 15*(3), 2137–2142.
40. Evlyukhin, A. B., Reinhardt, C., & Chichkov, B. N. (2011). Multipole light scattering by nonspherical nanoparticles in the discrete dipole approximation. *Physical Review B, 84*(23), 235429.
41. Solomon, M. L., et al. (2018). Enantiospecific optical enhancement of chiral sensing and separation with dielectric Metasurfaces. *ACS Photonics, 6*(1), 43–49.

42. Takechi, H., et al. (2011). Chiroptical measurement of chiral aggregates at liquid-liquid interface in centrifugal liquid membrane cell by Mueller matrix and conventional circular dichroism methods. *Molecules, 16*(5), 3636–3647.
43. Helgert, C., et al. (2011). Chiral metamaterial composed of three-dimensional plasmonic nanostructures. *Nano Letters, 11*(10), 4400–4404.
44. Esposito, M., et al. (2015). Tailoring chiro-optical effects by helical nanowire arrangement. *Nanoscale, 7*(43), 18081–18088.
45. Singh, R., et al. (2009). Terahertz metamaterial with asymmetric transmission. *Physical Review B, 80*(15), 153104.
46. Song, K., et al. (2013). A frequency-tunable 90°-polarization rotation device using composite chiral metamaterials. *Applied Physics Letters, 103*(10), 101908.
47. Plum, E., Fedotov, V. A., & Zheludev, N. I. (2009). Planar metamaterial with transmission and reflection that depend on the direction of incidence. *Applied Physics Letters, 94*(13), 131901.
48. Fedotov, V. A., et al. (2007). Asymmetric transmission of light and enantiomerically sensitive plasmon resonance in planar chiral nanostructures. *Nano Letters, 7*(7), 1996–1999.
49. Li, Z., et al. (2016). Tunable dual-band asymmetric transmission for circularly polarized waves with graphene planar chiral metasurfaces. *Optics Letters, 41*(13), 3142–3145.
50. Han, J., et al. (2011). An ultrathin twist-structure polarization transformer based on fish-scale metallic wires. *Applied Physics Letters, 98*(15), 151908.
51. Gansel, J. K., et al. (2012). Tapered gold-helix metamaterials as improved circular polarizers. *Applied Physics Letters, 100*(10), 101109.
52. Pan, C., et al. (2014). Broadband asymmetric transmission of optical waves from spiral plasmonic metamaterials. *Applied Physics Letters, 104*(12), 121112.
53. Wang, Y., et al. (2016). Direct and indirect coupling mechanisms in a chiral plasmonic system. *Journal of Physics D: Applied Physics, 49*(40), 405104.
54. Bai, Y., et al. (2018). Asymmetric transmission of a planar metamaterial induced by symmetry breaking. *Journal of Physics. Condensed Matter, 30*(11), 114001.
55. Bai, Y., et al. (2018). Splitting an asymmetric transmission peak by introducing magnetic-dipole oscillation on gold film. *Optical Materials Express, 8*(9), 2743.
56. Aba, T., et al. (2018). Tunable asymmetric transmission through tilted rectangular nanohole arrays in a square lattice. *Optics Express, 26*(2), 1199–1205.
57. Hu, Z., et al. (2019). Plasmonic circular dichroism of gold nanoparticle based nanostructures. *Advanced Optical Materials, 7*(10), 1801590.
58. Kraust, J. (1949). The helical antenna*. *Proceedings of the IEEE, 37*, 263–272.
59. Esposito, M., et al. (2014). Nanoscale 3D chiral Plasmonic helices with circular dichroism at visible frequencies. *ACS Photonics, 2*(1), 105–114.
60. Wang, T., et al. (2017). Circular dichroism of a tilted U-shaped nanostructure. *Optics Letters, 42*(14), 2842–2845.
61. He, Y., et al. (2014). Tunable three-dimensional helically stacked plasmonic layers on nanosphere monolayers. *Nano Letters, 14*(4), 1976–1981.
62. Wang, Y., et al. (2016). Plasmonic chirality of L-shaped nanostructure composed of two slices with different thickness. *Optics Express, 24*(3), 2307–2317.
63. Ullah, H., et al. (2020). Giant circular dichroism of chiral L-shaped nanostructure coupled with achiral nanorod: Anomalous behavior of multipolar and dipolar resonant modes. *Nanotechnology, 31*(27), 275205.
64. Tang, B., et al. (2017). Chiral-selective Plasmonic Metasurface absorbers operating at visible frequencies. *IEEE Photonics Technology Letters, 29*(3), 295–298.
65. Yang, Z.-J., et al. (2016). Enhanced chiral response from the Fabry–Perot cavity coupled metasurfaces. *Chinese Physics B, 25*(8), 084201.
66. Li, J., et al. (2015). Nanoplasmonic sensors with various photonic coupling effects for detecting different targets. *The Journal of Physical Chemistry C, 119*(52), 29116–29122.
67. Bai, Y., et al. (2020). Increasing the circular dichroism of the planar chiral nanostructure by inducing coupling between the coverage layer and the planar nanostructure. *Optics Express, 28*(14), 20563–20572.

68. Decker, M., et al. (2009). Strong optical activity from twisted-cross photonic metamaterials. *Optics Letters, 34*(16), 2501–2503.
69. Decker, M., et al. (2010). Twisted split-ring-resonator photonic metamaterial with huge optical activity. *Optics Letters, 35*(10), 1593–1595.
70. Wang, Y., et al. (2019). Strong circular dichroism enhancement by plasmonic coupling between graphene and h-shaped chiral nanostructure. *Optics Express, 27*(23), 33869–33879.
71. Narushima, T., & Okamoto, H. (2013). Circular dichroism nano-imaging of two-dimensional chiral metal nanostructures. *Physical Chemistry Chemical Physics, 15*(33), 13805–13809.
72. Phua, W. K., et al. (2015). Study of circular dichroism modes through decomposition of planar nanostructures. *Plasmonics, 11*(2), 449–457.
73. Zhao, Y., et al. (2017). Chirality detection of enantiomers using twisted optical metamaterials. *Nature Communications, 8*, 14180.
74. Wu, X., et al. (2013). Unexpected chirality of nanoparticle dimers and ultrasensitive chiroplasmonic bioanalysis. *Journal of the American Chemical Society, 135*(49), 18629–18636.
75. Tullius, R., et al. (2015). "Superchiral" spectroscopy: Detection of protein higher order hierarchical structure with chiral plasmonic nanostructures. *Journal of the American Chemical Society, 137*(26), 8380–8383.
76. Qu, Y., et al. (2020). Chiral near-fields induced by plasmonic chiral conic nanoshell metallic nanostructure for sensitive biomolecule detection. *The Journal of Physical Chemistry C, 124*(25), 13912–13919.
77. Kumar, J., & Liz-Marzán, L. M. (2019). Recent advances in chiral plasmonics – Towards biomedical applications. *Bulletin of the Chemical Society of Japan, 92*(1), 30–37.
78. Hendry, E., et al. (2010). Ultrasensitive detection and characterization of biomolecules using superchiral fields. *Nature Nanotechnology, 5*(11), 783–787.
79. Ben-Moshe, A., et al. (2013). Chirality and chiroptical effects in inorganic nanocrystal systems with plasmon and exciton resonances. *Chemical Society Reviews, 42*(16), 7028–7041.
80. Wang, Y., et al. (2017). Induced chirality in micron wave through electromagnetic coupling between chiral molecules and graphene nanostructures. *Carbon, 120*, 203–208.
81. Govorov, A. O. (2011). Plasmon-induced circular dichroism of a chiral molecule in the vicinity of metal nanocrystals. Application to various geometries. *The Journal of Physical Chemistry C, 115*(16), 7914–7923.
82. Abudukelimu, A., et al. (2019). The causality of circular dichroism inducement by isotropic and anisotropic chiral molecules. *Journal of Physics D: Applied Physics, 52*(30), 305306.
83. Bochenkov, V. E., & Shabatina, T. I. (2018). Chiral plasmonic biosensors. *Biosensors (Basel), 8*(4), 120.
84. Nesterov, M. L., et al. (2016). The role of plasmon-generated near fields for enhanced circular dichroism spectroscopy. *ACS Photonics, 3*(4), 578–583.
85. Le Ru, E. C., & Etchegoin, P. G. (2013). Quantifying SERS enhancements. *MRS Bulletin, 38*(8), 631–640.
86. Vestler, D., et al. (2018). Circular dichroism enhancement in plasmonic nanorod metamaterials. *Optics Express, 26*(14), 17841–17848.
87. Lu, F., et al. (2013). Discrete nanocubes as plasmonic reporters of molecular chirality. *Nano Letters, 13*(7), 3145–3151.
88. Yao, Y., et al. (2014). Wide wavelength tuning of optical antennas on graphene with nanosecond response time. *Nano Letters, 14*(1), 214–219.
89. Liu, T., Yi, Z., & Xiao, S. (2017). Active control of near-field coupling in a terahertz metal-graphene metamaterial. *IEEE Photonics Technology Letters, 29*(22), 1998–2001.
90. Zhou, Y., et al. (2018). Tunable low loss 1D surface plasmons in InAs nanowires. *Advanced Materials, 30*(35), e1802551.
91. Yin, X., et al. (2015). Active chiral plasmonics. *Nano Letters, 15*(7), 4255–4260.
92. Tian, X., et al. (2018). Improving Luttinger-liquid plasmons in carbon nanotubes by chemical doping. *Nanoscale, 10*(14), 6288–6293.